

Robust Torque Vectoring Control

S. Kaspar* J. Ludwig* T. Bunte** S. Hohmann***

* *BMW Group Forschung und Technik, Munich, Germany (e-mail: Stephan.Kaspar, Julian.JL.Ludwig@bmw.de)*
** *Institute of System Dynamics and Control, DLR Oberpfaffenhofen, Germany (e-mail: Tilman.Buente@dlr.de).*
*** *Karlsruhe Institute of Technology, Karlsruhe, Germany (e-mail: soeren.hohmann@kit.edu)*

Abstract:

An investigation on the robustness of a torque vectoring control based on an inverse disturbance observer architecture for a rear wheel driven vehicle with electric single wheel drives is presented within this contribution. To ensure robust control parameters, specifications for eigenvalues (Γ -stability) and bounds on weighted sensitivity and complementary sensitivity functions in frequency domain (\mathcal{B} -stability) are formulated and transferred into parameter space. Simulation results show the effectiveness of the chosen controller design and parameter setup.

1. INTRODUCTION

Maximization of possible driving range is one of the key issues of electric vehicles. Therefore, large and heavy batteries need to be attached to the vehicle. Within the Project FAIR (Fahrwerk/Antrieb-Integration ins Rad, transl. chassis/drive integration into the wheel), the BMW Group Research and Technology together with its partners Schaeffler and the German Aerospace Center (DLR) made investigation how to perfectly integrate the batteries and the drive train into a vehicle to ideally utilize given installation space and the additional degrees of freedom given by the electric powertrain without using State-of-the-Art in-wheel motors. The outcome is a vehicle prototype based on a MINI Countryman with electric single rear wheel drives as shown in figure 1. The gearbox is not only used as housing for the gears, but for chassis functions as wheel guidance and suspension as well. The system combines the benefits of in-wheel-drives with its very little installation space requirements as well as the advantage of small unsprung masses of conventional drive trains. The inherent ability of free torque distribution (so-called torque vectoring) allows manipulation of the vehicle dynamics within wide ranges. The corresponding torque vectoring control needs to be robust w.r.t. large variations in longitudinal speed, payload and road adhesion and w.r.t unstructured uncertainty (unmodelled dynamics). This can be assured by the controller settings found in this contribution. The paper is organized as follows. In section 2, an overview of the control structure and related transfer functions is given. Section 3 is an explanation of the used parameter space approach and the problem specifications. Concrete formulation of the specifications, transfer into parameter space and the associated stability regions in parameter space is illustrated in chapter 4. Finally, the effectiveness and stability of the used controls is shown in section 5 via simulation results.

2. CONTROL ARCHITECTURE

The used control structure is called "Inverse Disturbance Observer (IDOB)", an overview of the architecture is given in figure 3. Within this paper, only a brief overview of the main aspects will be given. For a more specific description please refer to Bunte et al. (2014). The disturbance observer is a specific method to ensure robustness to both modelling errors and disturbance rejection (Ohnishi (1987) Umeno and Hori (1991)), and was successfully implemented in a variety of control applications such as high speed direct drive positioning (Kempf and Kobayashi (1999)), friction compensation (Güvenç and Srinivasan (1994)) and vehicle steering control (Bunte et al. (2002)). For realization of an effective torque vectoring control, we adopted the Inverse Disturbance Observer control structure after Bajcinca and Bunte (2005) due to its effectiveness and ease of practical application.

Input signal is the angle of the steered front wheels δ induced by the driver (and the vehicles' longitudinal speed, which is treated as slowly changing parameter). The desired yaw rate is calculated through G_{ref} , the transfer function of a single track model (cp. Appendix A). The reference value is computed by two decoupled parts to be able to independently adjust steady-state and transient behaviour. The control structure is shown in figure 2 and

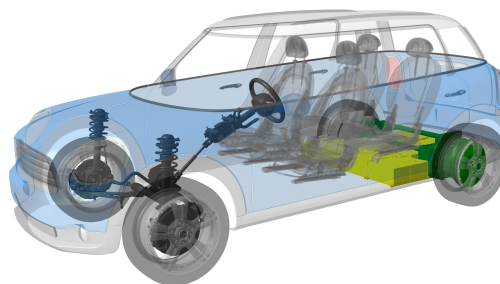


Fig. 1. Vehicle Prototype with electric single wheel drives attached to the rear wheel axle

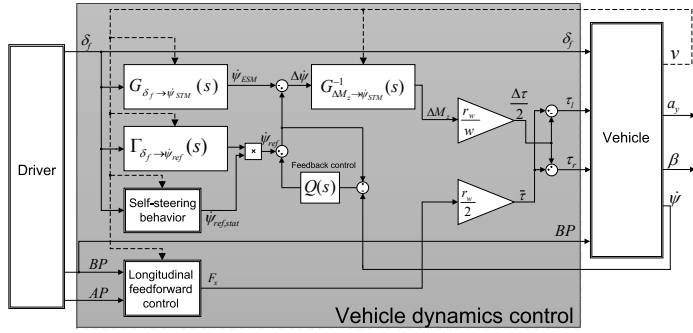


Fig. 2. Torque vectoring control structure [Bünthe et al. (2014)]

explained more in detail in Bünthe et al. (2014). Here, for the ease of understanding and readability, the desired transfer function is aggregated to G_{ref} (cp. figure 3). Since it is only necessary to add an additional yaw moment to receive desired yaw dynamics as the vehicle itself yaws due to the steering wheel angle, the unmodified yaw rate (without torque vectoring) is calculated by the (single track model based) transfer function $G_{\delta_f \rightarrow \psi_{STM}}(s) = G_{Mod,\delta}$ and subtracted from the desired yaw rate. The transfer function $G_{\Delta M_z \rightarrow \psi_{STM}}(s) = G_{Mod,M}$ describes the single track model relation between the additional yaw moment ΔM_z and the vehicle's yaw rate. As this transfer function has a relative degree of one and hence can not be inverted exactly, an additional fast time constant T_{real} needs to be added for realization of the inverse transfer function $G_{Mod,M}^{-1}$. T_{real} should be chosen very small for best accuracy. Here, as the sampling rate is 100 Hz, T_{real} is chosen to be 0.02. $G_{Fzg,\delta}$ and $G_{Fzg,M}$ are the transfer functions of the real vehicle from steer angle respectively additional yaw moment to yaw rate. The resulting relation between steer angle δ and yaw rate $\dot{\psi}$ can be calculated as

$$G_{\delta\dot{\psi}} = \frac{G_{Fzg,M}G_{Mod,M}^{-1}G_{Ref}}{1 - Q(1 - G_{Fzg,M}G_{Mod,M}^{-1})} + \frac{(Q - 1)(G_{Fzg,M}G_{Mod,M}^{-1}G_{Mod,\delta} - G_{Fzg,\delta})}{1 - Q(1 - G_{Fzg,M}G_{Mod,M}^{-1})} \quad (1)$$

There are two possibilities to achieve the desired behaviour: Either perfect inversion (which is not possible, as mentioned before), leading to $G_{Fzg,M}G_{Mod,M}^{-1} = 1$, or $Q = 1$. either way, the result is:

$$G_{\delta\dot{\psi}} = G_{Ref}. \quad (2)$$

Considering external disturbances d like different friction coefficients or side wind, the effect on the yaw rate can be calculated by the sensitivity function

$$G_{d\dot{\psi}} = \frac{1 - Q}{1 - Q(1 - G_{Fzg,M}G_{Mod,M}^{-1})}. \quad (3)$$

The desired value for Q is one again to eliminate the influence of disturbances on the yaw rate.

For sensor noise rejection (noise signal n), the complementary sensitivity function can be calculated as:

$$G_{n\dot{\psi}} = \frac{QG_{Fzg,M}G_{Mod,M}^{-1}}{1 - Q(1 - G_{Fzg,M}G_{Mod,M}^{-1})} \quad (4)$$

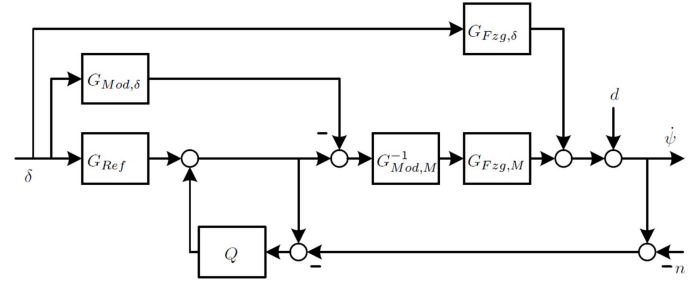


Fig. 3. Control architecture

For repressing influences caused by sensor noise, the desired value for Q is zero. Taking all requirements into account and assuming relevant sensor noise at high frequencies while main disturbances are as well as the driver input on lower frequencies, all demands can be fulfilled by choosing Q as a low pass filter. Within this contribution, Q is realised as a unity gain PT_1 filter:

$$Q(s) = \frac{1}{T_Q s + 1}. \quad (5)$$

Whenever approaching the system limits (actuator saturation and/or friction limits), anti-wind-up measures are made with Q being lowered to avoid improper wheel torque demands. Furthermore, an additional slip-controller is implemented for each wheel.

3. SPECIFICATIONS

Within this section, the investigated operating points and the general approach for evaluation of robust control parameters is presented.

3.1 Operating Points

As previously discussed, for modeling the vehicle yaw dynamics, single track model equations are employed. The dynamic behaviour of the single track model, as well as for the real vehicle, can vary within a wide range as many parameters can change during driving. The longitudinal speed can vary from zero up to the vehicles top speed which is limited to 42 m/s. The cornering stiffnesses c_f and c_r can exhibit large variations as well as the friction coefficient μ between road and tires can be subject to large variations. To ensure stable behavior during all driving situations, several operating points are investigated, which are marked as cross markers in figure 4. The maximum value for μ is 1.0, which is valid for all speeds. The lower friction coefficient is chosen according to Bünthe et al. (2002) to be 0.2 (icy road) for low speed up to 0.7 for high speed (wet asphalt). At this point, one particular operating point (high speed on low friction coefficient) is chosen to demonstrate the approach for determination of stable parameter sets. The same procedure is done subsequently

for all six operation points. In section 4.5, the located stability domains for each operating point are mapped to generate a global valid proposition.

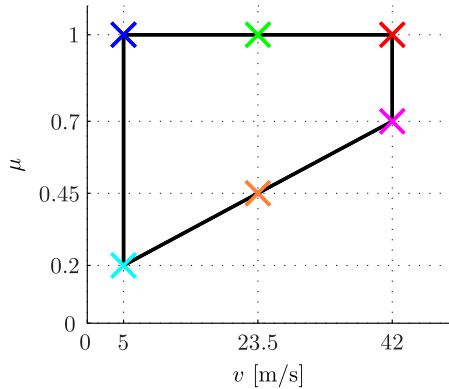


Fig. 4. Operating points

3.2 Γ -stability

Hurwitz-Stability is assured if all poles of the system $G(s)$ lie in the complex left half plane \mathbb{C}^- (Puente León et al. (2011)), i.e.

$$\text{poles}\{G(s)\} \subset \mathbb{C}^-. \quad (6)$$

Γ -stability is the demand on the poles, not only to be in the left plane, but furthermore to be located within a certain area Γ which itself is part of \mathbb{C}^- , i.e.

$$\text{poles}\{G(s)\} \subset \Gamma \subset \mathbb{C}^-. \quad (7)$$

In this way, not only stability of the system is provided, but also performance specifications can be formulated. All poles of the system need to be and stay within this region Γ for all frequencies so that the system is declared to be stable. Usually, three characteristic boundaries for formulation of the rim $\partial\Gamma$ are claimed:

- The first specification is the shifted imaginary axis to the left to guarantee that the system's settling time is limited.
- Two lines of constant damping ensure a specified minimum damping ratio.
- A circle with radius R , centered at the origin, to limit the systems' maximum frequency.

Figure 5 shows the exemplary shape of Γ as cut set of the particular boundaries.

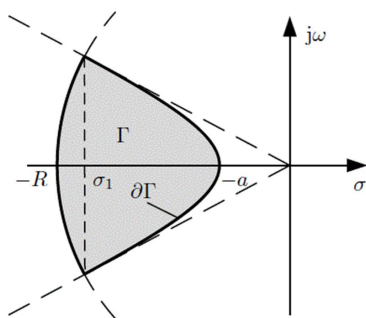


Fig. 5. Exemplary Γ -specifications in eigenvalue domain

3.3 \mathcal{B} -Stability

For the \mathcal{B} -stability criterion, the frequency response magnitude (FRM) of the system is investigated. As before for Γ -specifications, a desired area is defined and the system is determined to be \mathcal{B} -stable if its frequency response magnitude (FRM) stays within those limits. Figure 6 shows two different specifications: The magnitude boundary can either be chosen as a closed continuous curve, e.g. the FRM of a transfer function, or as piecewise defined region. The \mathcal{B} -stability criterion for a linear time invariant system $G(s)$ is defined as

$$|G(j\omega)| \subset \mathcal{B}, \quad \forall \omega \in [\omega^-, \omega^+] \quad (8)$$

where \mathcal{B} is the region within the border $\partial\mathcal{B}$.

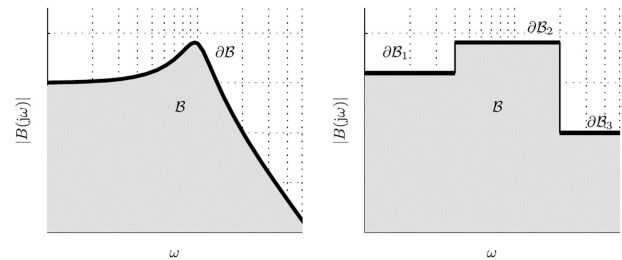


Fig. 6. Closed (left) and piecewise (right) defined \mathcal{B} -boundaries

4. SPECIFICATIONS IN PARAMETER SPACE

Within this section, reasonable boundaries to obtain robust parameters for Γ and \mathcal{B} stability are chosen. For parameter space, the two most influential parameters for the vehicle are investigated: μ_r , which is the adjusted friction coefficient of the single track models in the controller, and T_Q , the time constant of the low pass feedback filter Q .

4.1 Gamma Stability

As mentioned before, the vehicle response is dependent on the actual driving situation. Γ -specifications have been adopted to this by the specifications:

- The imaginary axis is shifted by -2 to ensure fast system response analogous to Bünthe et al. (2002).
- The damping ratio is chosen according to the actual operating point. As the minimum requirement for the control structure is to at least not worsen the damping ratio of the uncontrolled vehicle, the damping ratio of the unmodified single track model for the particular driving situation is chosen.
- For system limitations with respect to the Nyquist Theorem, the maximum frequency was limited to 50Hz (which correlates 100π rad/s). Analyses demonstrated that this boundary is never violated, hence for better illustration, the radius of the circle is chosen to be 60 rad/s.

A visualization of the specification for several operating points is illustrated in figure 7 (left), the colors correspond to the respective operating points in Figure 4. The related robust stability region in parameter space for the chosen exemplary driving situation (high speed, low friction) is given on the right side. Stable parameter sets are marked magenta.

4.2 Disturbance Stability

Decisive disturbances are assumed to be on low frequencies, hence a first-order high pass filter (9) FRM is chosen as specification for disturbance rejection (see figure 8 left).

$$\partial\mathcal{B}_S = K_{BS} \frac{T_{BS}s}{T_{BS}s + 1} \quad (9)$$

Assessment of the needed parameters K_{BS} and T_{BS} is made in two steps: Firstly, high frequencies are limited to a maximum amplification of 10%, which leads to $K_{BS} = 1.1$. Secondly, the cut-off frequency needs to be determined. In order to avoid the excitation of the eigen frequency of the vehicle, the cut-off frequency of the reference high pass is chosen to be 1 Hz higher than the damped eigen frequency of the single track model. The corresponding robust stability region in parameter space is illustrated in Figure 8 right.

4.3 Stability against measurement noise

The complementary sensitivity function (4) describes the impact of measurement noise on the resulting yaw rate. It is assumed that the yaw rate sensor is considerable exact for low frequencies while disturbances and errors occur for higher frequencies. Nevertheless, measurement errors in lower frequency ranges should not be amplified too much. Hence, a second-order lowpass filter is chosen as boundary $\partial\mathcal{B}_{T,1}$:

$$\partial\mathcal{B}_{T,1} = K_{BT} \frac{1}{(T_{BT}s + 1)(T_{BT}s + 1)} \quad (10)$$

The time constant $T_{BT} = 0.21$ is chosen according to the specifications of the yaw rate sensor (postulated accuracy until 13 Hz), the amplification for pass band is limited to 1% ($K_{BT} = 1.01$). Figure 9 shows the chosen boundaries

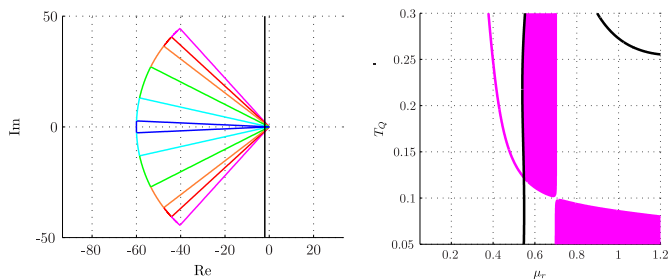


Fig. 7. Specifications of the Γ -domain (left) and the related mapping in parameter space (right)

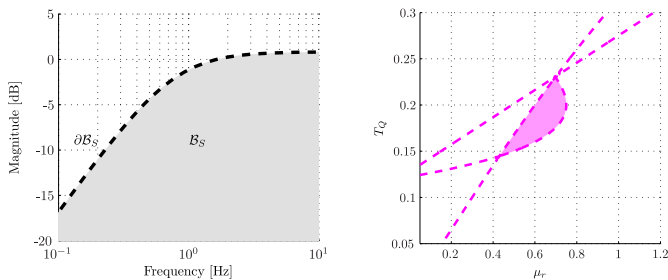


Fig. 8. \mathcal{B} -specifications for external disturbances (left) and corresponding stable parameter space regions (right)

for FRM (left) and the found stable domain in parameter space (right).

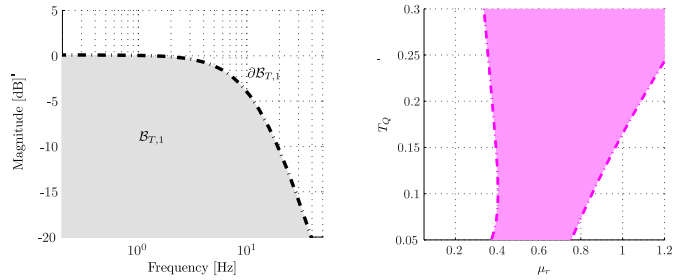


Fig. 9. \mathcal{B} -specifications for sensor noise (left) and corresponding stable parameter space regions (right)

4.4 Stability against unstructured uncertainties

Until here, assumptions were made that parameters of the vehicle were correctly modelled. For the real vehicle, there will always be deviations between modelled behavior and real vehicle behavior due to model imprecisions or changing parameters. A main advantage of the \mathcal{B} -space approach is that it is possible to determine the effects on stability of such unstructured uncertainties. It is assumed that the model is quite accurate for low frequencies and becomes more and more imprecise the higher the frequency is. Therefore, 10 % magnitude uncertainty was selected for low frequencies and 500 % uncertainty for high frequencies, with a transition frequency of 6 Hz between low gain and high gain. The corresponding curve of the boundary condition is shown in figure 10 (left), related stability regions in parameter space are illustrated (right).

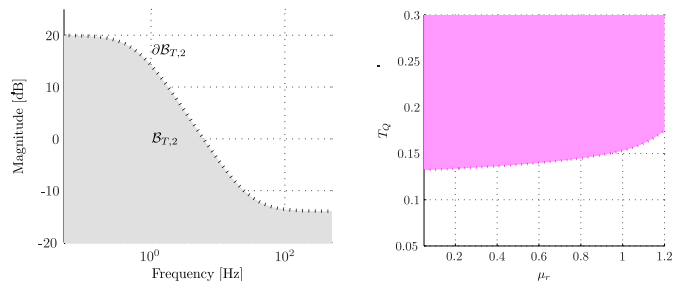


Fig. 10. \mathcal{B} -specifications for unstructured uncertainties (left) and corresponding stable parameter space regions (right)

4.5 Stability regions

The final step for evaluation of stable controller parameters T_Q and μ_r for this exemplary point of operation is to synthesise the particular stable regions to find the final parameter set which is stable and fulfills all requirements as it is done in figure 11 (left). Merging all specifications and the resulting stable regions in parameter space (Γ -stability: solid lines; Disturbance stability: dashed lines; Measure noise stability: dash-dotted lines; Stability against unstructured uncertainties: dotted lines), the magenta area is found as solution to fulfill all requirements. The summary for all points of operation is shown on the right side (colors corresponding to the operation points as defined

in figure 4). According to the identified stability regions, the following assessments can be made:

- It is possible to find a global valid value for the time constant T_Q of the first order feedback lowpass filter Q which ensures all specifications stay within desired limits. For further investigation, T_Q is chosen to be 0.2 from here on. This result corresponds perfectly to the results found during real vehicle test driving on low friction coefficient, cp. Bünthe et al. (2014).
- It is not possible to find a global value for μ_r which guarantees fulfillment of the requirements.
- The friction coefficient must not be overrated, but it can be underestimated (by 10%, if $T_Q = 0.2$ is chosen).

For further investigation, it is assumed that friction estimation, suitable to above mentioned boundaries, is available from here on.

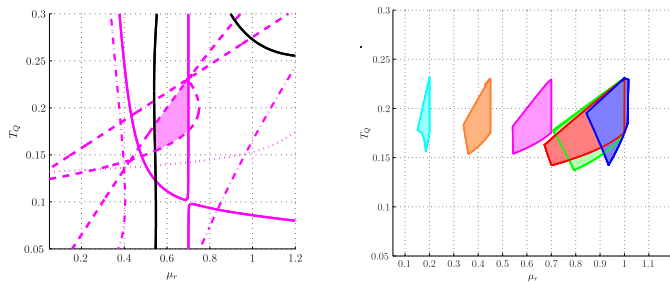


Fig. 11. Synthesis of all requirements for $v=150\text{km/h}$, $\mu=0.7$ (left) and all operating points (right)

5. SIMULATION RESULTS

Based on the findings above, the time constant T_Q is chosen to be 0.2, the friction value is supposed to be known for each operating point. To show the effectiveness and robustness of the control architecture against variation of other parameters than μ and v , simulations with different setups for several driving maneuvers are made. As before, the operating points shown in figure 4 are investigated. The simulation environment is a matlab/simulink based validated full vehicle model with 5 bodies and 16 degrees of freedom. The tire forces are calculated via Pacejka's well-known magic formula (Pacejka (2005)). For this contribution, a straight line maneuver with steady-state side wind at a certain part of the track as external disturbance is chosen, exemplarily shown here for the operating point of high speed on the lower friction coefficient ($\mu=0.7$). To demonstrate the robustness against model uncertainties, four different load setups are chosen, while the controller settings remain unchanged:

- w1 : weight distribution as defined for controller design, with two passengers (68kg each) in the front and 7 kg luggage per person in the trunk.
- w2 : light scenario; only the vehicle and one driver with 68 kg payload, no luggage.
- w3 : heavy weight scenario; maximum rear axle load, front axle load as much as possible to reach the permitted overall weight limits. This results in 115kg extra axle load on the front and 330kg on the rear axle.

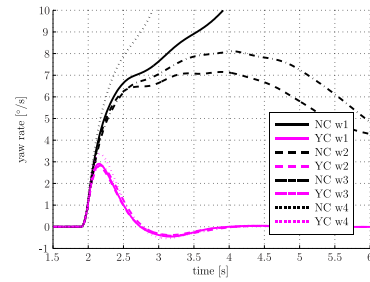


Fig. 12. Simulation Results: Yaw rate without (NC) and with yaw control (YC) for different axle load distributions

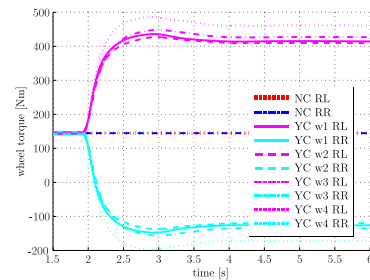


Fig. 13. Simulation Results: Wheel torques without (NC) and with yaw control (YC) for different axle load distributions

- w4 : tail-heavy scenario; rear axle load at maximum, front axle load at minimum with only the driver, no other front-seat passenger and no luggage in the front.

The vehicle is driving straight with steady-state longitudinal velocity. At $t=1.9\text{s}$, the vehicle reaches a field with steady-state side wind. In Rompe and Heißing (1984) it is suggested that the side wind velocity should not be more than 60% of the vehicle speed. Hence, 50% (21 m/s) was chosen here. Throttle and steering wheel angle are kept constant during the entire maneuver. As the average reaction time of the driver is one second, it is important that the lateral deviation, as well as the yaw rate is compensated very fast before the driver is able to react. The simulation results for the yaw rate is given in figure 12. All uncontrolled vehicles (NC) show large lateral deviations and high yaw rates. Considerable distinctions between the different setups can be found: w2 and w3 manage to lower or at least stabilize the yaw rate (even on a high and potentially dangerous level), while w1 and w4 drift away. The controlled vehicles (YC) show consistent stable behaviour: The yaw rate is stabilized, the settling time is less than one second, hence, within the reaction time of the driver. Corresponding wheel torques are given in figure 13. As the side winds' direction is from right to left, wheel torque is shifted to the left to compensate the unwanted yawing. The torque values of w3 and w4 are more or less on the same level, while the tail-heavy car needs to shift more wheel torque to stabilize the car. Nevertheless, all wheel torques are within the power range of the wheel drives and the influence of the disturbance is eliminated. Simulation results for the other operating points show analogous behaviour.

6. CONCLUSION

Within this contribution, the robust design of a model-based inverse disturbance observer control structure for wheel torque allocation of an electric vehicle with single wheel drives attached to the rear wheels was introduced. Eigenvalue specifications (Γ -stability) and bounds on sensitivity and complementary sensitivity functions (\mathcal{B} -stability) in the FRM were formulated for evaluation of stable controller parameters. It was possible to find a global valid parameter T_Q which fulfills all requirements. This was not possible for the friction coefficient used in the controller; nevertheless, the required accuracy of friction estimation was evaluated. The effectiveness and robustness of the yaw controller with respect to other parameter variations for several operating points on the μ - v -plane was investigated and shown in simulation results for an exemplary operating point. The findings within this paper correspond perfectly to the experiences during real vehicle tests, for steady state as well as for evasive maneuvers (cp. Bünte et al. (2014)).

ACKNOWLEDGEMENTS

The FAIR project received financial support by Bayerische Forschungsförderung (grant AZ-840-08, cf. Leonhardt (2013)). The authors want to especially thank Dr. Dirk Odenthal from the BMW Group for his great support.

REFERENCES

- Ackermann, J., Blue, P., Bünte, T., Güvenc, L., Kaesbauer, D., Kordt, M., Muhler, M., and Odenthal, D. (2002). *Robust Control: The Parameter Space Approach*. Springer, London.
- Ackermann, J., Bartlett, A., Kaesbauer, D., Siemel, W., and Steinhauser, R. (1993). *Robust control*. Springer.
- Bajcinca, N. and Bünte, T. (2005). A novel control structure for dynamic inversion and tracking tasks. In *Proc. 16th IFAC World Congress*. Prague.
- Bünte, T., Kaspar, S., Hohman, S., and Brembeck, J. (2014). Inverse model based torque vectoring control for a rear wheel driven battery electric vehicle. *IFAC World Congress 2014*. Submitted to the IFAC World Congress 2014.
- Bünte, T., Odenthal, D., Aksun-Güvenç, B., and Güvenç, L. (2002). Robust vehicle steering control design based on the disturbance observer. *Annual reviews in control*, 26(1), 139–149.
- Güvenç, L. and Srinivasan, K. (1994). Friction compensation and evaluation for a force control application. *Mechanical Systems and Signal Processing*, 8(6), 623–638.
- Kempf, C.J. and Kobayashi, S. (1999). Disturbance observer and feedforward design for a high-speed direct-drive positioning table. *Control Systems Technology, IEEE Transactions on*, 7(5), 513–526.
- Leonhardt, D. (ed.) (2013). *Jahresbericht 2012*. Bayerische Forschungsförderung.
- Ohnishi, K. (1987). A new servo method in mechatronics. *Trans. Jpn. Soc. Elect. Eng.*, 107, 83–86.
- Pacejka, H. (2005). *Tyre and vehicle dynamics*. Elsevier.
- Puente León, F., Kiencke, U., and Jäkel, H. (2011). Signale und systeme. *Signale und Systeme*.
- Riekert, P. and Schunck, T.E. (1940). Zur fahrmechanik des gummibereiften kraftfahrzeugs. *Ingenieur-Archiv*, 11(3), 210–224.
- Rompe, K. and Heiβing, B. (1984). *Objektive Testverfahren für die Fahreigenschaften von Kraftfahrzeugen*. Verlag TUV Rheinland GmbH Köln.
- Umeno, T. and Hori, Y. (1991). Robust speed control of dc servomotors using modern two degrees-of-freedom controller design. *Industrial Electronics, IEEE Transactions on*, 38(5), 363–368.

Appendix A. SINGLE TRACK MODEL

The well-known single track model (Riekert and Schunck (1940)) is used for modelling the vehicle yaw dynamics.

Its major variables and geometric parameters are:

- F_f/F_r : lateral wheel force at front (rear) wheel
- r : yaw rate
- β : chassis side slip angle at center of gravity (CG)
- v : magnitude of velocity vector at CG ($v > 0$, $\dot{v} = 0$)
- l_f/l_r : distance between front/rear axle and CG
- δ : steer angle of the front wheels
- m : total weight of the vehicle
- J : moment of inertia

Assuming small steer angles δ and small values for the side slip angle β , the linearized equations of motion are (Ackermann et al. (1993), Ackermann et al. (2002))

$$\left[\frac{mv(\dot{\beta} + r)}{ml_f l_r \dot{r}} \right] = \left[\frac{F_f + F_r}{F_f l_f - F_r l_r} \right] \quad (\text{A.1})$$

The tire force characteristics are linearized as

$$F_f(\alpha_f) = \mu c_f \alpha_f, \quad F_r(\alpha_r) = \mu c_r \alpha_r \quad (\text{A.2})$$

with the tire cornering stiffnesses c_f , c_r , the road adhesion factor μ and the tire side slip angles

$$\alpha_f = \delta - \left(\beta + \frac{l_f}{v} r \right) \quad (\text{A.3})$$

$$\alpha_r = - \left(\beta - \frac{l_r}{v} r \right) \quad (\text{A.4})$$

The transfer function from the front steer angle δ to the yaw rate r can be computed from (A.1)-(A.4):

$$G(s) = \frac{r(s)}{\delta(s)} = \frac{b_0 + b_1 s}{a_0 + a_1 s + a_2 s^2} \quad (\text{A.5})$$

with

- b_0 : $c_f c_r (l_f + l_r) v$
- b_1 : $c_f l_f m v^2$
- a_0 : $c_f c_r (l_f + l_r)^2 + (c_r l_r - c_f l_f) m v^2$
- a_1 : $(c_f (J + l_f^2 m) + c_r (J + l_r^2 m)) v$
- a_2 : $J m v^2$

The nominal values for the linearized single track model assumed in this contribution are $l_f = 1.55$ m, $l_r = 1.05$ m, $m = 1843$ kg, $J = 2626$ kgm², $c_f = 98000$ N/rad and $c_r = 150000$ N/rad.